

http://pubs.acs.org/journal/aelccp

# Upcycling of Spent LiNi<sub>0.33</sub>Co<sub>0.33</sub>Mn<sub>0.33</sub>O<sub>2</sub> to Single-Crystal Ni-Rich Cathodes Using Lean Precursors

Hongpeng Gao, Qizhang Yan, Duc Tran, Xiaolu Yu, Haodong Liu, Mingqian Li, Weikang Li, Junlin Wu, Wei Tang, Varun Gupta, Jian Luo, and Zheng Chen\*



ABSTRACT: Lithium-ion batteries (LIBs) are widely applied in portable electronics, electric vehicles (EVs), and grid storage systems. They need sustainable end-of-life battery management to reduce greenhouse emissions and resource consumption to create a low-carbon future. Here, we report an efficient upcycling method, converting spent polycrystalline LiNi<sub>0.33</sub>Co<sub>0.33</sub>Mn<sub>0.33</sub>O<sub>2</sub> (NCM111) up to single-crystal LiNi<sub>0.8</sub>Co<sub>0.1</sub>Mn<sub>0.1</sub>O<sub>2</sub> (NCM811) with lean input of precursors. A systematic investigation of the microstructure evolution in the upcycling process revealed an Ostwald ripening phenomenon during the particle transformation. Optimizing the sintering temperature and reaction time results in single-crystal particles showing uniform Ni element distribution and valence state, clean surface, and tunable sizes. Particularly, these structural features endow upcycled NCM811 with improved performance (198 mAh/g at C/10 and 173 mAh/g at 1 C) compared to commercial polycrystals while maintaining good cycling stability. This work demonstrates a feasible pathway toward affordable and efficient upcycling in today's sustainable development of NCM cells, which paves the way for the next-generation LIB recycling and upcycling.

apid growth in lithium-ion battery (LIB) production has served the rising demand for portable electronics, electric vehicles (EVs), and grid energy storage systems. Since the 2010s, an expeditious growth of EVs has been accompanied by tumbling prices and enormous enthusiasm for LIBs. As these EVs inevitably reach their end of life (EOL), a large number of spent LIBs would be generated after their service life of up to 8–10 years. For these EOL batteries from the primary applications with 80% of their original capacity, one potential solution is to reuse them in less demanding applications, such as utility and backup power storage devices, where they can extend their lifespan. Nonetheless, this approach postpones the eventual recycling of LIBs. It remains a critical and pressing issue to recycle all EOL LIBs.

**D-NCM 111** 

Hydrometallurgical and pyrometallurgical processes have been adopted in the state-of-the-art LIB recycling industry. Intensive energy consumption and caustic processes, such as high-temperature smelting, acid leaching, and chemical precipitation, are inevitably associated with heavy  ${\rm CO_2}$  emission and other waste generation. On the other hand, the emerging direct recycling technology has attracted increasing attention due to the minimum energy consumption and maximum potential profit compared with traditional hydrometallurgical and pyrometallurgical recycling methods.  $^{7-10}$  Extensive efforts have been devoted to healing the structure

Received: July 16, 2023 Accepted: August 31, 2023 Published: September 13, 2023

with tunable size





ACS Energy Letters http://pubs.acs.org/journal/aelccp Letter

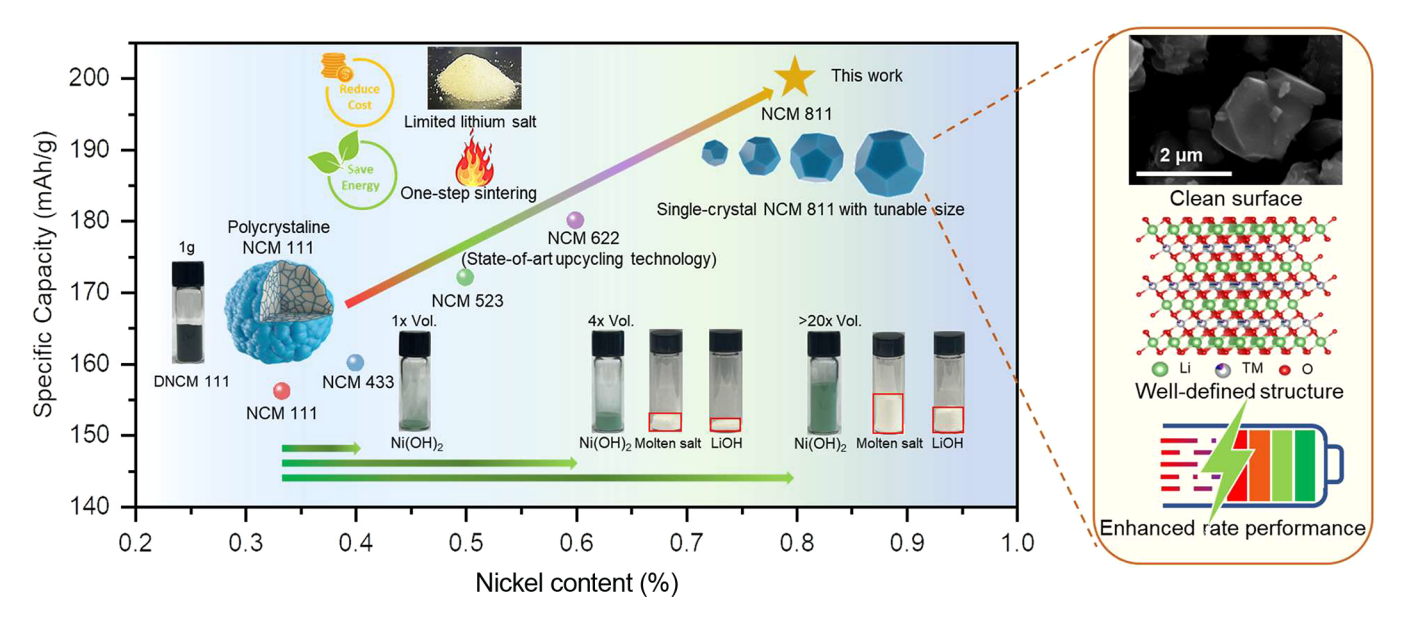


Figure 1. Schematic illustration of the direct upcycling method. The spent (delithiated) polycrystalline NCM particles (e.g., D-NCM111) are mixed with Ni-containing precursors (e.g., Ni(OH)<sub>2</sub>) by ball milling to form a homogeneous mixture, which is subject to relithiation with a limited amount of LiOH (by the sintering process) to obtain single-crystal NCM particles with a clean surface (no lithium salt residuals), well-defined structure, and enhanced rate performance. The amount of molten salt as a comparison is based on the state-of-art upcycling method in Ma et al.'s work. <sup>23</sup>

and composition defects of cathode active materials from spent LIBs, including solid-state sintering, 11 hydrothermal treatment, 8,12,13 ionothermal process, 14 redox mediation, 15 and molten eutectic salt relithiation 16 followed by a short annealing process. While solid-state sintering by mixing all precursors in a stoichiometric ratio seems to be a simple strategy, determining the amount of supplementary Li source is challenging for the mixed waste streams with spent LIBs with a wide range of states of health (SOH). By comparison, some self-saturated relithiation strategies have demonstrated high effectiveness in direct recycling without considering the SOH variation. 9,10,16–18

However, with the growing demands for high-energy-density LIBs, improving the performance of spent cathode active materials beyond the original pristine materials via recycling processes remains challenging as a critical milestone in the next-generation battery recycling.<sup>19</sup> In addition, single-crystal LiNi<sub>x</sub>Co<sub>v</sub>Mn<sub>1-x-v</sub>O<sub>2</sub> (NCM) cathodes have attracted increasing attention due to their superior structural stability compared with conventional polycrystalline particles.<sup>20</sup> As the accumulation of lattice strain and lattice distortion are susceptible in the polycrystalline particles due to the grain boundary evolution,<sup>21</sup> an effective direct approach to eliminate grain boundary fracture is to convert polycrystalline into singlecrystal domains, delivering superior kinetics and rate capability with significant integrity improvement with optimized size and morphology control.<sup>22</sup> Recently, a molten salt method based on a LiOH-Li<sub>2</sub>SO<sub>4</sub> salt mixture has been demonstrated to upgrade polycrystalline NCM 111<sup>23</sup> and NCM 532<sup>24</sup> into single-crystal NCM 622. This concept has also been illustrated to convert spent polycrystal LiNi<sub>0.88</sub>Co<sub>0.095</sub>Al<sub>0.025</sub>O<sub>2</sub> (NCA) into regenerated single crystals with same composition by a LiOH-Na<sub>2</sub>SO<sub>4</sub> eutectic molten salt system.<sup>25</sup> Moreover, a reciprocal ternary molten salt system of LiNO<sub>3</sub>-NaCl has been developed for upcycling spent NCM 111 into NCM 622.<sup>26</sup> At the same time, producing high-performance nickel-rich

cathodes (Ni >80%) has garnered significant attention due to their high energy output. In this regard, upgrading spent NCM 111 into single-crystal NCM 811 (or even higher Ni) is being considered as one of the ultimate solutions to avoid the multistep high-temperature calcination process by using excess lithium salt or a molten-salt flux method.<sup>27</sup> However, upcycling low-nickel cathodes to NCM811 remains a difficult task.

Herein, we report an efficient method to upgrade polycrystalline delithiated NCM 111 (D-NCM 111) into single-crystal NCM 811 with LiOH as a single supplementary source of lithium. The universality of this simple method was further demonstrated in synthesizing single-crystal NCM 433 and 622 by tuning the precursor ratios. We found that the Ostwald ripening phenomenon, occurring during flux growth of oxides when merging D-NCM with the Ni precursor, played a dominant role in determining particle morphology. Various characterization methods were applied to examine the uniformity of the Ni valence and distribution within the single-crystal particle. These upcycled single-crystal NMC showed outstanding electrochemical performance compared to the polycrystalline counterparts. Particularly, the resulting upcycled NCM 811 exhibited a significant improvement in its rate capability with good cycling stability, surpassing the performance of the original polycrystalline NCM 811. This effective direct upcycling method with limited Li salt, avoiding excess molten salt flux, significantly reduces the overall cost, as well as simplifies the recycling process, which provides a feasible pathway to scalable direct upcycling.

There is a growing consensus that increasing the nickel content is a direct way to boost the specific capacity of the NCM cathodes, which can also be applied to recycling/upcycling areas. In Figure 1, we show an efficient and versatile method to upgrade the polycrystalline D-NCM 111 to higher nickel NCM with single-crystal morphology control using a limited Li supplementary source. The SEM images of D-NCM 111 and the Ni(OH)<sub>2</sub> precursor are shown in Figure S1a,b.

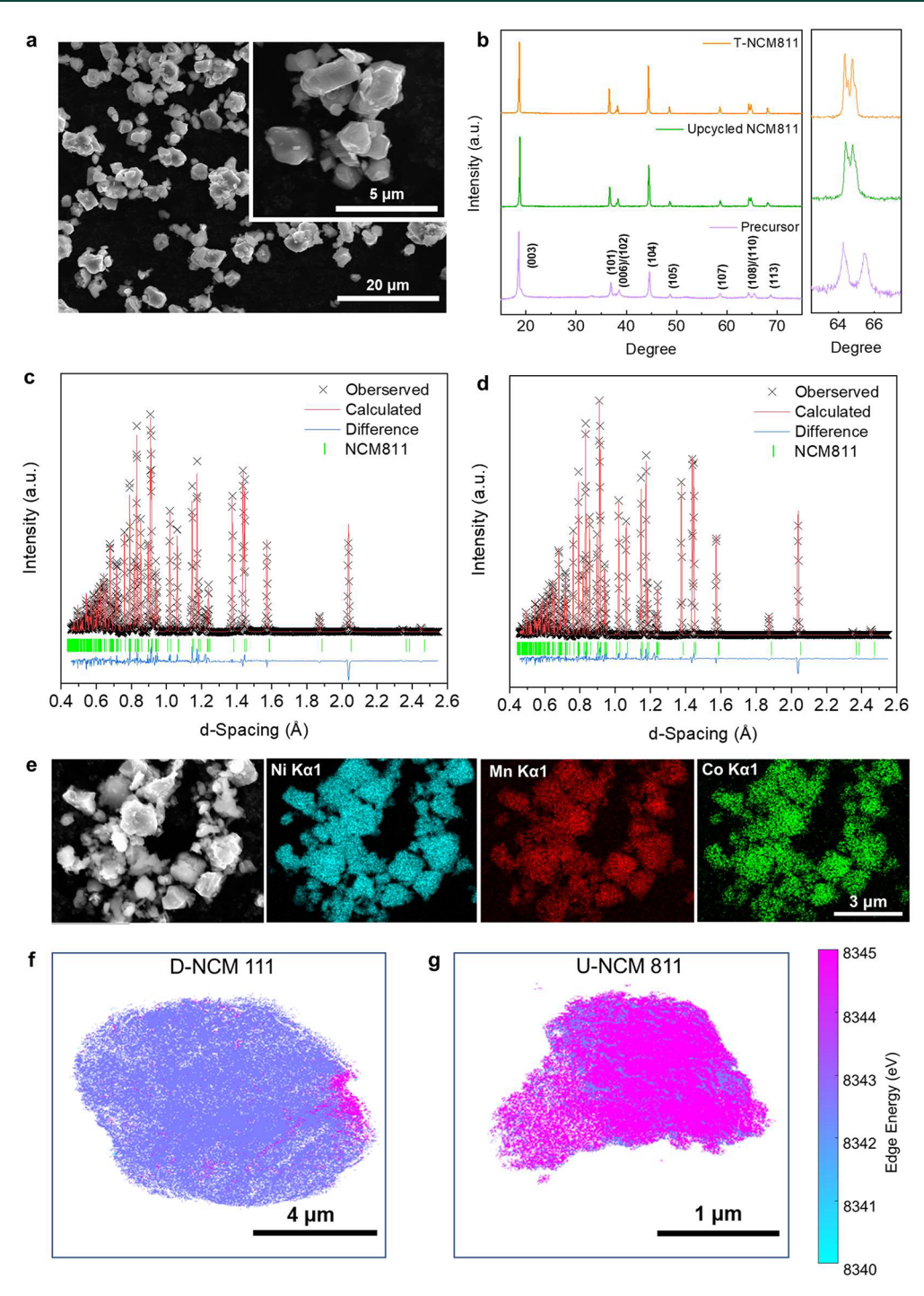


Figure 2. Phase determination and bulk information on nickel distribution of upcycled NCM 811. (a) SEM images and size distribution of U-NCM 811 synthesized under optimized conditions. (b) XRD patterns of U-NCM 811, T-NCM 811, and precursors. Neutron diffraction patterns of (c) U-NCM 811 and (d) T-NCM 811. (e) SEM-EDS images of U-NCM 811. 2D XANES mapping image of Ni in (f) U-NCM 811 and (g) D-NCM 111.

The morphology evolution reveals the transformation of polycrystalline particles to single-crystal particles. To achieve such a transformation, D-NCM 111 was first pulverized into primary grains via ball milling with the Ni(OH)<sub>2</sub> precursor, facilitating the extra Ni to diffuse into the NCM bulk phase. The homogeneous precursor (Figure S1c) was then subjected to a relithiation sintering step with 10% molar excess LiOH (to compensate for Li loss during the sintering step). A TGA-DSC analysis (Figure S2) illustrates the compositional evolution during the sintering process. A temperature hold at 480 °C for

3 h is applied to form a uniform LiOH solution with D-NCM and decomposed Ni(OH)<sub>2</sub> precursor. Following long-term sintering at high temperature, the fully lithiated single-crystal NCM 811 was obtained with no significant residual lithium salt on the surface. Similar methods can be applied to synthesize NCM 433 and 622 with good control of composition (Table S1) and phase purity (Figures S4 and S5). The corresponding samples under the optimal conditions are denoted as "U-NCM 433", "U-NCM 622", and "U-NCM 811", respectively.

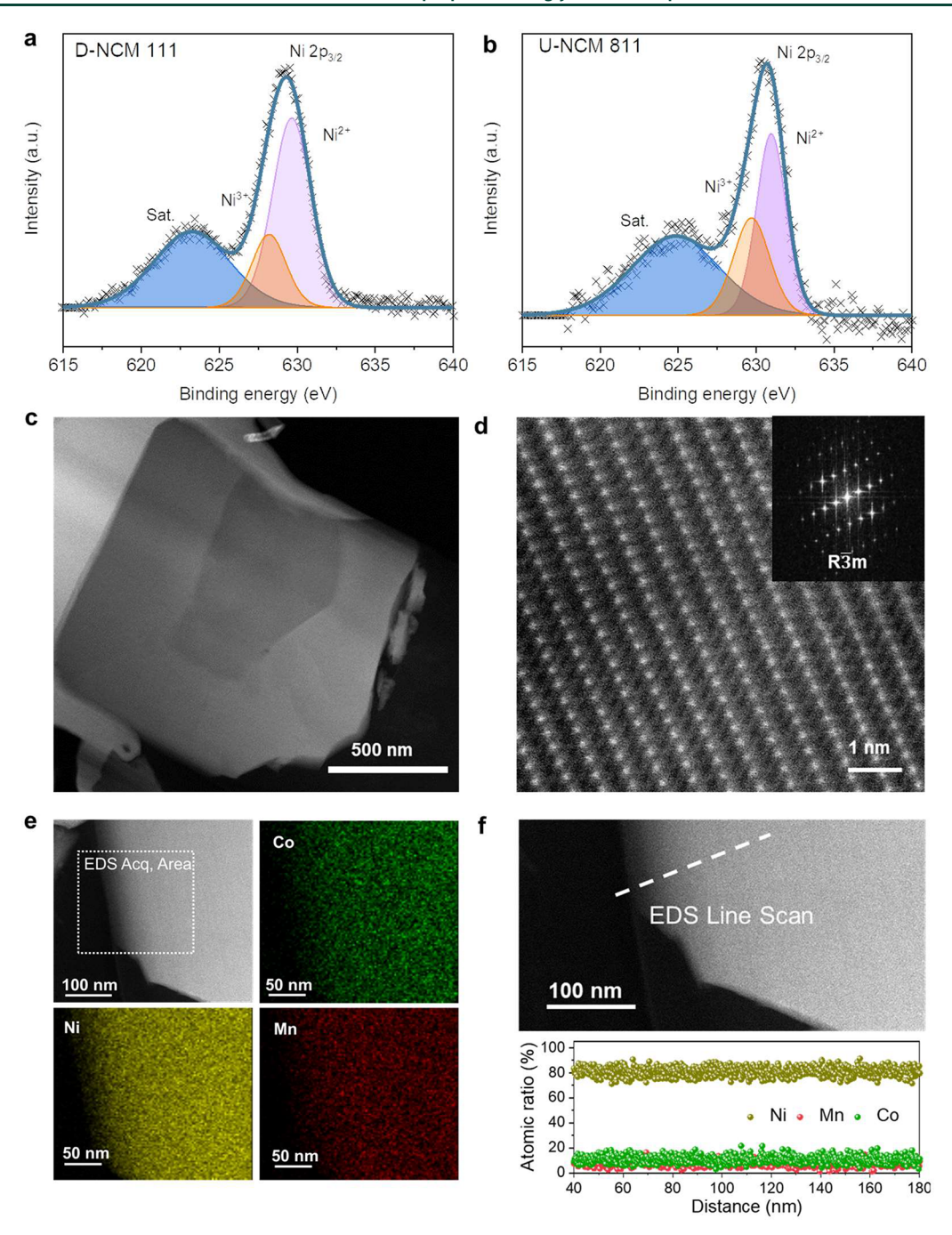


Figure 3. Microstructure and valence uniformity analyses of upcycled NCM 811. XPS spectra of (a) D-NCM 111 and (b) U-NCM 811. (c) Cross-section image of U-NCM 811. (d) HAADF-STEM image of upcycled NCM 811 with an inserted image of the FFT pattern. (e) TEM-EDS mapping of Ni, Co, and Mn. (f) EDS linear scanning with inserted elemental distribution intensity.

Compared with single-crystal NCM 622 obtained using an excess amount of molten salt flux of a Li mixture reported in recent works, <sup>23,24,26</sup> our lean LiOH approach enabled a better control of homogeneity as it is challenging to upgrade into single-crystal NCM 811 from the same starting material, D-NCM 111, with a large excess of Li salt, which also involves a large amount of transition-metal diffusion between metal precursors and the existing NCM host. As shown in Figure 1, more than 20× or 4× the volume of Ni(OH)<sub>2</sub> is required to reach the compositional formula for the final NCM811 product compared with NCM 433 or NCM 622 upcycling. More importantly, instead of using a large amount of mixed lithium salts to form the molten salt system, our direct

upgrading process utilizes a minimum amount of a single lithium salt (LiOH) to compensate the lithium loss in spent NCM and to react with newly added Ni precursor to form the desired Ni-rich NCM single crystals with high uniformity and tunable particle sizes. Our work demonstrated such a simple yet efficient method to upgrade NCM 111 into single-crystal NCM 811 with high elemental integrity and good electrochemical performance without any excess molten salt flux, which is critical for low-cost and scalable upcycling. Particularly, in large-scale operation this lean salt upcycling process will significantly reduce the water and energy usage for washing and reclaiming the extra Li.

The ability to control the size of the upcycled particles was investigated by tuning the sintering conditions. This process has revealed the occurrence of the well-known Ostwald ripening phenomenon, which is caused by variations in the solubilities of smaller and larger particles in the surrounding medium. It affects the diffusion of Ni into D-NCM 111, merging in the mixture of Ni(OH)<sub>2</sub> and LiOH. By extending the sintering time from 10 to 15 h at 900 °C, an obvious growth trend of primary particle sizes has been observed in "U-NCM 811-900-15h" with D50 sizes of 1.8, 2.1, and "U-NCM 811-900-15h" with D50 sizes of 1.8, 2.1, and 2.5  $\mu$ m, respectively (Figure S3). Additionally, the smallest (1.6  $\mu$ m) and largest (4.9  $\mu$ m) D50 sizes are obtained for U-NCM 811-850-10h and U-NCM 811-925-15h.

The morphology dependence on temperature can be ascribed to the higher solubility and mobility of the reactive components, allowing Ni diffusion and lithiation at a higher temperature. These manners of crystal growth have been observed in the flux growth of oxides, suggesting that the crystal size increases with the reaction time and holding temperature. Thus, through optimization of the sintering duration and temperature, we were able to exert control over the morphology of the upcycled NCM 811 material. The conversion of particles and their morphology change were thus featured as the Ostwald ripening phenomenon, which occurs during the flux growth of oxides when D-NCM particles merge and grow at the expense of the Ni precursor via dissolution and precipitation.

With the aforementioned direct upcycling method, the Nirich NCM single crystals are obtained with the desired compositions, confirmed by inductively coupled plasma mass spectrometry (ICP-MS) (Table S1). Note that 10% Lideficient D-NCM 111 (Li<sub>0.901</sub>Ni<sub>0.334</sub>Co<sub>0.335</sub>Mn<sub>0.331</sub>O<sub>2</sub>) was converted into fully lithiated NCM primary particles  $(Li_{1.025}Ni_{0.377}Co_{0.309}Mn_{0.314}O_2, Li_{1.061}Ni_{0.599}Co_{0.202}Mn_{0.207}O_2,$ and  $Li_{1.064}Ni_{0.801}Co_{0.097}Mn_{0.102}O_2$ ) in the form of single-crystal particles. According to a Brunauer-Emmett-Teller (BET) analysis (Table S2), U-NCM 811 shows a relatively higher surface area (1.74 m<sup>2</sup>/g) than that of polycrystalline T-NCM 811(1.20 m<sup>2</sup>/g), which is expected from its smaller particle size. To illustrate the effectiveness of our developed synthesis method, SEM images and XRD patterns of U-NCM 811 with optimized synthesis conditions are shown in Figure 2a,b. Meanwhile, Figures S4 and S5 illustrate the XRD patterns of other upcycled cathode samples, including both NCM 433 and NCM 622. Rietveld refinement was performed on all of the XRD patterns using the GSAS software with EXPGUI as the graphic user interface (Table S3). The standard pattern of a hexagonal  $\alpha$ -NaFeO<sub>2</sub> type structure with the R3m space group was validated in all samples without detectable phase impurities. The peak positions are well matched in all regenerated samples and the virgin polycrystalline NCM sample (T-NCM 433, T-NCM 622, and T-NCM 811), indicating that a pure high-Ni phase was successfully constructed. Moreover, the separation of (108)/(110) peaks became narrower when the Ni content increased in NCM, indicating the smaller c/a ratio in a hexagonal lattice.<sup>31</sup> The regenerated samples maintain the same peak separation with T-NCM433, T-NCM622, and T-NCM811 while the precursor samples have larger distances. The refinement results show that the c-axis lattice parameter (14.257 Å in T-NCM 111, 14.248 Å in U-NCM 433, 14.198 Å in U-NCM 622, 14.179 Å in U-NCM 811) of the NCM cathodes decreases, while the a-axis

parameter and lattice volume increase with the increase in the Ni content in the structure of the cathodes (2.859 Å in T-NCM 111, 2.867 Å in U-NCM 433, 2.871 Å in U-NCM 622, 2.874 Å in U-NCM 811) (Table S2). This can be attributed to the increased proportion of Ni<sup>3+</sup> ions and the simultaneous decrease in the concentration of Mn<sup>4+</sup> ions. Turthermore, the peak intensity ratio of I(003)/I(104) was above 1.85 in single-crystal samples compared to 1.44 in the pristine polycrystalline particles, which indicates a highly ordered lattice structure and lower Li/Ni mixing in single-crystal particles. The structure and lower Li/Ni mixing in single-crystal particles.

To further quantify the occupancy of Li sites and the percentage of Li/Ni antisite defects in the lattice, neutron diffraction was conducted on T-NCM 811 and U-NCM 811 (Figure 3a,b). Both samples demonstrate the O3-type layered α-NaFeO<sub>2</sub> structure, which consists of a closely packed oxygen array occupying the 6c sites. Li and transition metals (Ni, Co, and Mn) occupy the octahedral sites along the (111) plane, named 3a and 3b sites.<sup>35</sup> Typically, the Li/Ni antisite defects are composed of Li<sup>+</sup> and Ni<sup>2+</sup> due to their closer radius (0.76 Å for Li<sup>+</sup>, 0.69 Å for Ni<sup>2+</sup>).<sup>36</sup> According to the Rietveld refinement results given in Table S2, the upcycled NCM 811 contains less oxygen loss and less Ni<sup>2+</sup> compared with pristine NCM 811 due to the highly ordered structure inhibiting oxygen release. Hence, a lower Li/Ni mixing (3.54%) is observed in U-NCM 811 compared with 3.97% in T-NCM 811.

To confirm the uniformity of the transition-metal distribution in the U-NCM 811 sample, SEM-EDS was performed, and the related mappings are shown in Figure 2e. It is apparent that Ni, Co, and Mn are uniformly distributed along with the whole single-crystal particles. Similarly, the elemental distribution in upcycled NCM 433 and NCM 622 was also confirmed by SEM-EDS as shown in Figures S6 and S7, respectively, showing a uniform composition. Moreover, 3D tomography by transmission X-ray microscopy (TXM) and 2D X-ray absorption near-edge structure (XANES) mapping with a resolution of 28.7 nm per pixel were performed for a detailed investigation of the Ni valence distribution to reveal the elemental uniformity with high resolution. Figure S8a,b demonstrates the volume renderings of a primary particle from U-NCM 811 and D-NCM 111. The spherical D-NCM111 particle with secondary structure is >5  $\mu$ m in diameter, while the single-crystal U-NCM 811 is  $\sim$ 1.8  $\mu$ m with an anomalous shape. The 2D XANES mapping illustrates that the near-edge energy of Ni shifts to a higher energy with good uniformity after the upcycling process (Figure 2f,g). Therefore, a well-defined bulk structure characterized by a highly uniform Ni distribution was achieved through this simple sintering method with limited lithium source, resulting in upcycled single-crystal NCM 811 products.

To investigate the valence distribution of transition metals from the upcycled cathode material, XPS was performed on upcycled NCM 811 and D-NCM 111. The fitted Ni 2p<sub>3/2</sub> spectra in Figure 3a illustrates an non-negligible amount of Ni<sup>3+</sup> observed in D-NCM 111 due to a significant lithium deficiency in D-NCM 111. Figure 3b reveals a higher Ni<sup>3+</sup>/Ni<sup>2+</sup> ratio in upcycled NCM 811 in a fully lithiated status, suggesting that the average valence of Ni increases when its content increases from 33% in D-NCM 111 to 80% in U-NCM 811. The XPS results are consistent with the observations from 2D XANES mapping.

To further understand the microstructure of upcycled materials, the FIB lamella of U-NCM 811 was prepared and

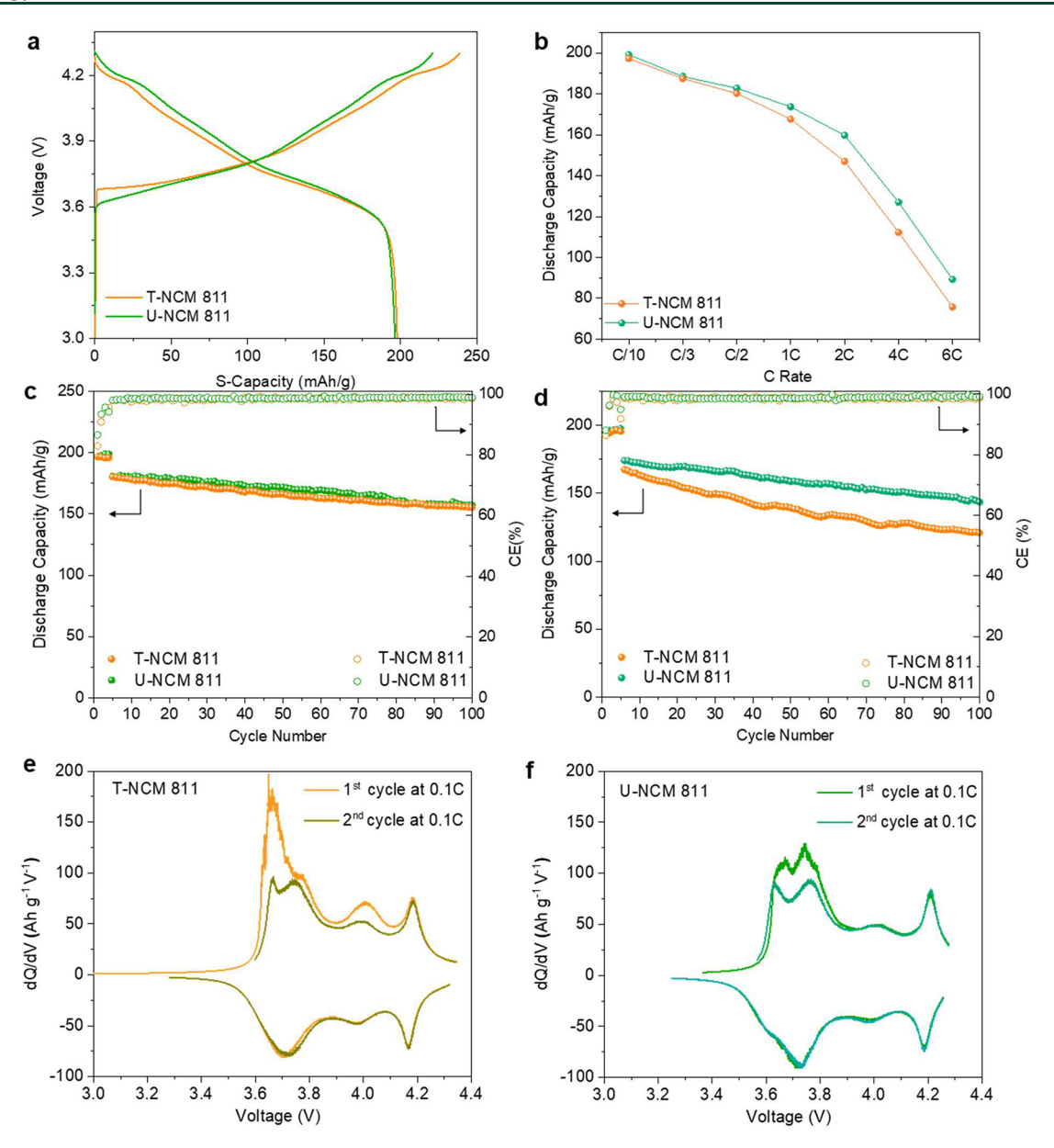


Figure 4. Electrochemical performance evaluation of upcycled materials. (a) Voltage profile at 0.1 C and (b) rate performance of T-NCM 811 and U-NCM 811. Cycling performance of T-NCM 811 and U-NCM 811 at (c) C/3 and 1 C cycling. dQ/dV plots of (e) U-NCM 811 and (f) T-NCM 811 at the first two activation cycles.

examined by STEM. Figure 3c shows the cross-sectional view of U-NCM 811 without any cavities, cracks, or clear grain boundaries. The high-resolution high-angle annular dark-field (HAADF)-STEM images with a fast Fourier transform (FFT) pattern again confirm the pure phase of  $\alpha$ -NaFeO<sub>2</sub>-type layered structures (Figure 3b). EDS mapping illustrates the uniform local distribution of Ni, Mn and Co at tens of nanometers scale (Figure 3c). The linear scanning validates the distribution of Ni, Mn, and Co with an exact 8:1:1 ratio with high uniformity in the grain of interest (Figure 3d).

The electrochemical performance of the pristine and upcycled NMC811 cells was evaluated by half cells at a potential between 2.8 and 4.3 V (versus Li/Li<sup>+</sup>). U-NCM 811 exhibits a similar specific discharge capacity at the first C/10 cycle (~198 mAh/g) and similar retention under C/3 cycling (Figure 4a–c) compared to the pristine sample. Moreover, Figure 4b illustrates the good rate performance of U-NCM 811

compared with the control sample. The 1 C/1 C cycling data reveal the significant improvement of structural durability in upcycled NCM 811, ascribed to the single-crystal structural integrity. U-NCM 811 shows 82.6% capacity retention after 100 cycles at 1 C/1 C cycling compared to only 72.2% retention in the pristine polycrystal sample (Figure 4d). To elaborate the difference between U-NCM 811 and T-NCM 811, the dQ/dV curves of the materials of interest are plotted in Figure 4e,f. As shown by the dQ/dV curves of the first two activation cycles, more irreversible capacity appears at ~3.8 V in upcycled single-crystal NCM while a significant irreversible capacity is observed at ~4.1 V in the pristine polycrystalline NCM. The extra charging capacity at a low state of charge (SOC) may be ascribed to the H1-M-H2 transition behavior in the single-crystal NCM 811, similar to that of LiNiO<sub>2</sub>, triggered by the rearrangement of Li/vacancy ordering.<sup>37</sup> A sluggish redox kinetics at a low SOC governed by ionic

transport at a low SOC in single crystals has also been confirmed by a recent study.  $^{38}$  Generally, the  $\mathrm{d}Q/\mathrm{d}V$  feature could show the H1-M-H2 transition existing in the first activation cycle at a slow rate. The smooth transition from H1 to H2 with M phase significantly reduces the strains and mechanical cracks on the grain boundaries raised by the coexistence of H1 and H2 phases.<sup>39</sup> It could be one of the important factors leading to the high stability of upcycled single-crystal particles at a high rate. On the hand, without a significant H1-M-H2 phase transition in lower Ni NCMs such as NCM 622, the difference in rate performance in upcycled NCM 622 and the pristine sample is not as significant as that in NCM 811, which is only 88.1% vs 81.0% after 100 cycles at 1 C/1 C (Figure S9). Both pristine and upcycled NCM 622 cathodes show similar dQ/dV curves at ~4.1 V (Figure S10), which demonstrates that the aforementioned phenomenon could not be observed in lower Ni NCMs.

In summary, we successfully demonstrated an effective strategy for direct upcycling of cathodes with minimized lithium source. Our approach involves converting spent polycrystalline NCM 111 into single-crystal high-Ni NCM particles with the desired Ni content and crystal size. We have also revealed a mechanism controlling the growth of NCM single crystals, supported by a thorough investigation of the size distribution and improved Ni content in the upcycled single-crystal NCM. By leveraging this straightforward process, the desired composition and high phase purity were achieved in the upcycled single-crystal particles, leading to good rate performance and improved cycling stability compared to the virgin polycrystalline cathodes. This study paves the way for a cost-effective and scalable upcycling approach for spent LIB materials, accommodating the diverse chemistries used in today's NCM cells.

# ASSOCIATED CONTENT

# **Solution** Supporting Information

The Supporting Information is available free of charge at https://pubs.acs.org/doi/10.1021/acsenergylett.3c01454.

Experimental section and supplementary figures (SEM images, size distributions, 3D-morphology patterns, Electrochemical performances, Rietveld refinement of the XRD patterns, and ICP measurement) (PDF)

### AUTHOR INFORMATION

## **Corresponding Author**

Zheng Chen — Program of Materials and Science Engineering, Department of Nano and Chemical Engineering, and Sustainable Power & Energy Center (SPEC), University of California San Diego, La Jolla, California 92093, United States; ◎ orcid.org/0000-0002-9186-4298; Email: zhengchen@eng.ucsd.edu

# Authors

Hongpeng Gao – Program of Materials and Science Engineering and Department of Nano and Chemical Engineering, University of California San Diego, La Jolla, California 92093, United States

Qizhang Yan — Program of Materials and Science Engineering and Department of Nano and Chemical Engineering, University of California San Diego, La Jolla, California 92093, United States

- Duc Tran Department of Nano and Chemical Engineering, University of California San Diego, La Jolla, California 92093, United States
- Xiaolu Yu Program of Materials and Science Engineering and Department of Nano and Chemical Engineering, University of California San Diego, La Jolla, California 92093, United States
- Haodong Liu Department of Nano and Chemical Engineering, University of California San Diego, La Jolla, California 92093, United States
- Mingqian Li Department of Nano and Chemical Engineering and Sustainable Power & Energy Center (SPEC), University of California San Diego, La Jolla, California 92093, United States
- Weikang Li Department of Nano and Chemical Engineering, University of California San Diego, La Jolla, California 92093, United States
- Junlin Wu Program of Materials and Science Engineering and Department of Nano and Chemical Engineering, University of California San Diego, La Jolla, California 92093, United States
- Wei Tang Department of Nano and Chemical Engineering, University of California San Diego, La Jolla, California 92093, United States
- Varun Gupta Program of Materials and Science Engineering and Department of Nano and Chemical Engineering, University of California San Diego, La Jolla, California 92093, United States; orcid.org/0000-0002-4976-8593
- Jian Luo Program of Materials and Science Engineering, Department of Nano and Chemical Engineering, and Sustainable Power & Energy Center (SPEC), University of California San Diego, La Jolla, California 92093, United States

Complete contact information is available at: https://pubs.acs.org/10.1021/acsenergylett.3c01454

## **Author Contributions**

H.G.: investigation, methodology, formal analysis, writing, visualization. Q.Y.: investigation, methodology, formal analysis. X.Y.: methodology, formal analysis. H.L.: methodology, formal analysis. M.L.: investigation, formal analysis. W.L.: formal analysis, writing. D.T.: formal analysis. J.W.: investigation. W.T.: investigation. V.G.: formal analysis. J.L.: resources, funding acquisition. Z.C.: conceptualization, investigation, methodology, formal analysis, resources, supervision, funding acquisition.

# Notes

The authors declare the following competing financial interest(s): U.S. Provisional Application Serial No. 63/536,890 associated with this work was filed through the UC San Diego Office of Innovation and Commercialization.

## ACKNOWLEDGMENTS

This work was supported by the US Department of Energy (DOE) via ReCell Center and the start-up fund support from the Jacob School of Engineering at UC San Diego. Q.Y. and J.L.'s contribution to the microscopy work was supported as part of the Center for Synthetic Control Across Length scales for Advancing Rechargeables (SCALAR), an Energy Frontier Research Center funded by the United States Department of Energy, Office of Science, Basic Energy Sciences, under Award No. DE-SC0019381. Part of this work used the UCSD-MTI

Battery Fabrication Facility and the UCSD-Arbin Battery Testing Facility. Neutron diffraction work was carried out at the Spallation Neutron Source (SNS), which is the US DOE user facility at the Oak Ridge National Laboratory, sponsored by the Scientific User Facilities Division, Office of Basic Energy Sciences (BES). Use of the Stanford Synchrotron Radiation Light source, SLAC National Accelerator Laboratory, is supported by the US Department of Energy, Office of Science, Office of Basic Energy Sciences, under Proposal No. S-XV-ST-5823. The authors acknowledge the use of a shared TEM facility at the UC Irvine Materials Research Institute (IMRI), which is supported in part by the National Science Foundation through the UC Irvine Materials Research Science and Engineering Center (UCI MRSEC DMR-2011967), as well as the Nano3/SDNI and IMCF facilities and instrumentation supported by the National Science Foundation (ECCS-1542148 and UCSD MRSEC DMR-2011924) at UC San Diego for specimen preparation.

# REFERENCES

- (1) Gil-Alana, L. A.; Monge, M. Lithium: Production and estimated consumption. Evidence of persistence. *Resources Policy* **2019**, *60*, 198–202.
- (2) Fan, E.; Li, L.; Wang, Z.; Lin, J.; Huang, Y.; Yao, Y.; Chen, R.; Wu, F. Sustainable Recycling Technology for Li-Ion Batteries and Beyond: Challenges and Future Prospects. *Chem. Rev.* **2020**, *120* (14), 7020–7063.
- (3) Chen, M.; Ma, X.; Chen, B.; Arsenault, R.; Karlson, P.; Simon, N.; Wang, Y. Recycling End-of-Life Electric Vehicle Lithium-Ion Batteries. *Joule* **2019**, 3 (11), 2622–2646.
- (4) Shahjalal, M.; Roy, P. K.; Shams, T.; Fly, A.; Chowdhury, J. I.; Ahmed, M. R.; Liu, K. A review on second-life of Li-ion batteries: prospects, challenges, and issues. *Energy* **2022**, *241*, No. 122881.
- (5) Abdelbaky, M.; Peeters, J. R.; Dewulf, W. On the influence of second use, future battery technologies, and battery lifetime on the maximum recycled content of future electric vehicle batteries in Europe. *Waste Management* 2021, 125, 1–9.
- (6) Geng, J.; Gao, S.; Sun, X.; Liu, Z.; Zhao, F.; Hao, H. Potential of electric vehicle batteries second use in energy storage systems: The case of China. *Energy* **2022**, *253*, No. 124159.
- (7) Harper, G.; Sommerville, R.; Kendrick, E.; Driscoll, L.; Slater, P.; Stolkin, R.; Walton, A.; Christensen, P.; Heidrich, O.; Lambert, S.; et al. Recycling lithium-ion batteries from electric vehicles. *Nature* **2019**, *575* (7781), 75–86.
- (8) Xu, P.; Yang, Z.; Yu, X.; Holoubek, J.; Gao, H.; Li, M.; Cai, G.; Bloom, I.; Liu, H.; Chen, Y.; An, K.; Pupek, K. Z.; Liu, P.; Chen, Z. Design and Optimization of the Direct Recycling of Spent Li-Ion Battery Cathode Materials. ACS Sustainable Chem. Eng. 2021, 9 (12), 4543–4553.
- (9) Xu, P.; Dai, Q.; Gao, H.; Liu, H.; Zhang, M.; Li, M.; Chen, Y.; An, K.; Meng, Y. S.; Liu, P.; Li, Y.; Spangenberger, J. S.; Gaines, L.; Lu, J.; Chen, Z. Efficient Direct Recycling of Lithium-Ion Battery Cathodes by Targeted Healing. *Joule* 2020, 4 (12), 2609–2626.
- (10) Gao, H.; Yan, Q.; Xu, P.; Liu, H.; Li, M.; Liu, P.; Luo, J.; Chen, Z. Efficient Direct Recycling of Degraded LiMn<sub>2</sub>O<sub>4</sub> Cathodes by One-Step Hydrothermal Relithiation. ACS Appl. Mater. Interfaces **2020**, 12 (46), 51546–51554.
- (11) Ma, T.; Guo, Z.; Shen, Z.; Wu, Q.; Li, Y.; Yang, G. Molten salt-assisted regeneration and characterization of submicron-sized LiNi<sub>0.5</sub>Co<sub>0.2</sub>Mn<sub>0.3</sub>O<sub>2</sub> crystals from spent lithium ion batteries. *J. Alloys Compd.* **2020**, 848, No. 156591.
- (12) Shi, Y.; Chen, G.; Liu, F.; Yue, X.; Chen, Z. Resolving the Compositional and Structural Defects of Degraded LiNi<sub>x</sub>Co<sub>y</sub>Mn<sub>z</sub>O<sub>2</sub> Particles to Directly Regenerate High-Performance Lithium-Ion Battery Cathodes. *ACS Energy Letters* **2018**, 3 (7), 1683–1692.
- (13) Yu, X.; Yu, S.; Yang, Z.; Gao, H.; Xu, P.; Cai, G.; Rose, S.; Brooks, C.; Liu, P.; Chen, Z. Achieving low-temperature hydro-

- thermal relithiation by redox mediation for direct recycling of spent lithium-ion battery cathodes. *Energy Storage Materials* **2022**, *51*, 54–62
- (14) Wang, T.; Luo, H.; Bai, Y.; Li, J.; Belharouak, I.; Dai, S. Direct Recycling of Spent NCM Cathodes through Ionothermal Lithiation. *Adv. Energy Mater.* **2020**, *10* (30), No. 2001204.
- (15) Park, K.; Yu, J.; Coyle, J.; Dai, Q.; Frisco, S.; Zhou, M.; Burrell, A. Direct cathode recycling of end-of-life Li-ion batteries enabled by redox mediation. *ACS Sustainable Chem. Eng.* **2021**, *9* (24), 8214–8221.
- (16) Shi, Y.; Zhang, M.; Meng, Y. S.; Chen, Z. Ambient-Pressure Relithiation of Degraded  $\text{Li}_x\text{Ni}_{0.5}\text{Co}_{0.2}\text{Mn}_{0.3}\text{O}_2$  (0 < x < 1) via Eutectic Solutions for Direct Regeneration of Lithium-Ion Battery Cathodes. *Adv. Energy Mater.* **2019**, *9* (20), No. 1900454.
- (17) Shi, Y.; Chen, G.; Chen, Z. Effective regeneration of LiCoO <sub>2</sub> from spent lithium-ion batteries: a direct approach towards high-performance active particles. *Green Chem.* **2018**, *20* (4), 851–862.
- (18) Jing, Q.; Zhang, J.; Liu, Y.; Zhang, W.; Chen, Y.; Wang, C. Direct Regeneration of Spent LiFePO<sub>4</sub> Cathode Material by a Green and Efficient One-Step Hydrothermal Method. *ACS Sustainable Chem. Eng.* **2020**, *8* (48), 17622–17628.
- (19) Zhang, R.; Meng, Z.; Ma, X.; Chen, M.; Chen, B.; Zheng, Y.; Yao, Z.; Vanaphuti, P.; Bong, S.; Yang, Z.; et al. Understanding fundamental effects of Cu impurity in different forms for recovered LiNi<sub>0.6</sub>Co<sub>0.2</sub>Mn<sub>0.2</sub>O<sub>2</sub> cathode materials. *Nano Energy* **2020**, *78*, No. 105214.
- (20) Zhang, F.; Lou, S.; Li, S.; Yu, Z.; Liu, Q.; Dai, A.; Cao, C.; Toney, M. F.; Ge, M.; Xiao, X.; Lee, W.-K.; Yao, Y.; Deng, J.; Liu, T.; Tang, Y.; Yin, G.; Lu, J.; Su, D.; Wang, J. Surface regulation enables high stability of single-crystal lithium-ion cathodes at high voltage. *Nat. Commun.* **2020**, *11* (1), 3050.
- (21) Qian, G.; Zhang, Y.; Li, L.; Zhang, R.; Xu, J.; Cheng, Z.; Xie, S.; Wang, H.; Rao, Q.; He, Y.; et al. Single-crystal nickel-rich layered-oxide battery cathode materials: synthesis, electrochemistry, and intragranular fracture. *Energy Storage Materials* **2020**, *27*, 140–149.
- (22) Trevisanello, E.; Ruess, R.; Conforto, G.; Richter, F. H.; Janek, J. Polycrystalline and Single Crystalline NCM Cathode Materials—Quantifying Particle Cracking, Active Surface Area, and Lithium Diffusion. *Adv. Energy Mater.* **2021**, *11* (18), No. 2003400.
- (23) Ma, X.; Hou, J.; Vanaphuti, P.; Yao, Z.; Fu, J.; Azhari, L.; Liu, Y.; Wang, Y. Direct upcycling of mixed Ni-lean polycrystals to single-crystal Ni-rich cathode materials. *Chem.* **2022**, 8 (7), 1944–1955.
- (24) Qian, G.; Li, Z.; Wang, Y.; Xie, X.; He, Y.; Li, J.; Zhu, Y.; Xie, S.; Cheng, Z.; Che, H.; Shen, Y.; Chen, L.; Huang, X.; Pianetta, P.; Ma, Z.-F.; Liu, Y.; Li, L. Value-creating upcycling of retired electric vehicle battery cathodes. *Cell Reports Physical Science* **2022**, 3 (2), No. 100741.
- (25) Qin, Z.; Zhang, Y.; Luo, W.; Zhang, T.; Wang, T.; Ni, L.; Wang, H.; Zhang, N.; Liu, X.; Zhou, J.; et al. A Universal Molten Salt Method for Direct Upcycling of Spent Ni-rich Cathode towards Single-crystalline Li-rich Cathode. *Angew. Chem.* **2023**, *135*, No. e202218672.
- (26) Wang, T.; Luo, H.; Fan, J.; Thapaliya, B. P.; Bai, Y.; Belharouak, I.; Dai, S. Flux upcycling of spent NMC 111 to nickel-rich NMC cathodes in reciprocal ternary molten salts. *iScience* **2022**, 25 (2), No. 103801.
- (27) Yoon, M.; Dong, Y.; Huang, Y.; Wang, B.; Kim, J.; Park, J.-S.; Hwang, J.; Park, J.; Kang, S. J.; Cho, J. Eutectic salt-assisted planetary centrifugal deagglomeration for single-crystalline cathode synthesis. *Nature Energy* **2023**, *8*, 1–10.
- (28) Kimijima, T.; Zettsu, N.; Yubuta, K.; Hirata, K.; Kami, K.; Teshima, K. Molybdate flux growth of idiomorphic Li (Ni  $_{1/3}$  Co  $_{1/3}$  Mn  $_{1/3}$ ) O  $_2$  single crystals and characterization of their capabilities as cathode materials for lithium-ion batteries. *Journal of Materials Chemistry A* **2016**, 4 (19), 7289–7296.
- (29) Zhu, X.; Zhou, J.; Jiang, M.; Xie, J.; Liang, S.; Li, S.; Liu, Z.; Zhu, Y.; Zhu, J.; Liu, Z. Molten Salt Synthesis of Bismuth Ferrite Nano- and Microcrystals and their Structural Characterization. *J. Am. Ceram. Soc.* **2014**, *97* (7), 2223–2232.

- (30) Park, J. H.; Lee, D. H.; Shin, H. S.; Lee, B. K. Transition of the Particle-Growth Mechanism with Temperature Variation in the Molten-Salt Method. *J. Am. Ceram. Soc.* **1996**, 79 (4), 1130–1132.
- (31) Wang, J.; Zhang, Z.; He, W.; Wang, Z.; Weng, S.; Li, Q.; Wang, X.; Barg, S.; Chen, L.; Li, H.; Wu, F. Fast charge storage kinetics by surface engineering for Ni-rich layered oxide cathodes. *Journal of Materials Chemistry A* **2023**, *11* (19), 10239–10253.
- (32) Zhu, J.; Chen, G. Single-crystal based studies for correlating the properties and high-voltage performance of Li  $[Ni_xMn_yCo_{1-x-y}]O_2$  cathodes. *Journal of Materials Chemistry A* **2019**, 7 (10), 5463–5474.
- (33) Lee, K.-S.; Myung, S.-T.; Amine, K.; Yashiro, H.; Sun, Y.-K. Structural and Electrochemical Properties of Layered Li [Ni<sub>1-2x</sub>Co<sub>x</sub>Mn<sub>x</sub>]O<sub>2</sub> (x= 0.1-0.3) Positive Electrode Materials for Li-Ion Batteries. *J. Electrochem. Soc.* **2007**, *154* (10), A971.
- (34) Kosova, N.; Devyatkina, E.; Kaichev, V. Optimization of Ni<sup>2+</sup>/Ni<sup>3+</sup> ratio in layered Li(Ni,Mn,Co)O<sub>2</sub> cathodes for better electrochemistry. *J. Power Sources* **2007**, *174*, 965–969.
- (35) Tsebesebe, N.; Kgatwane, K.; Ledwaba, R.; Ngoepe, P. Investigating the Structural and Electronic Properties of LiMO<sub>2</sub> (M: Mn, Ni, Co) as Potential Cathode Materials: A DFT Study. *Journal of Physics: Conference Series* **2022**, 2298, No. 012010.
- (36) Wang, C.; Wang, R.; Huang, Z.; Chu, M.; Ji, W.; Chen, Z.; Zhang, T.; Zhai, J.; Lu, H.; Deng, S.; Chen, J.; He, L.; Liang, T.; Wang, F.; Wang, J.; Deng, Y.; Cai, W.; Xiao, Y. Unveiling the migration behavior of lithium ions in NCM/Graphite full cell via in operando neutron diffraction. *Energy Storage Materials* **2022**, *44*, 1–9.
- (37) Chien, P. H.; Wu, X.; Song, B.; Yang, Z.; Waters, C. K.; Everett, M. S.; Lin, F.; Du, Z.; Liu, J. New insights into structural evolution of LiNiO<sub>2</sub> revealed by operando neutron diffraction. *Batteries & Supercaps* **2021**, *4* (11), 1701–1707.
- (38) Ge, M.; Wi, S.; Liu, X.; Bai, J.; Ehrlich, S.; Lu, D.; Lee, W. K.; Chen, Z.; Wang, F. Kinetic Limitations in Single-Crystal High-Nickel Cathodes. *Angew. Chem., Int. Ed.* **2021**, *60* (32), 17350–17355.
- (39) Zhu, H.; Tang, Y.; Wiaderek, K. M.; Borkiewicz, O. J.; Ren, Y.; Zhang, J.; Ren, J.; Fan, L.; Li, C. C.; Li, D.; Wang, X.-L.; Liu, Q. Spontaneous Strain Buffer Enables Superior Cycling Stability in Single-Crystal Nickel-Rich NCM Cathode. *Nano Lett.* **2021**, *21* (23), 9997–10005.